MOLECULAR AND CELLULAR BIOLOGY, May 2007, p. 3470–3480 Vol. 27, No. 9
0270-7306/07/$08.00+0 doi:10.1128/MCB.00659-06

Targeting of the ETS Factor Gabpα Disrupts Neuromuscular Junction Synaptic Function▽§

Debra A. O'Leary,[1]† Peter G. Noakes,[2] Nick A. Lavidis,[2] Ismail Kola,[1]‡ Paul J. Hertzog,[1]* and Sika Ristevski[1]

Centre for Functional Genomics and Human Disease, Monash Institute of Medical Research, Monash University, Clayton, Victoria 3168, Australia,[1] and School of Biomedical Sciences, University of Queensland, St. Lucia, Queensland 4072, Australia[2]

Received 15 April 2006/Returned for modification 10 June 2006/Accepted 30 October 2006

The GA-binding protein (GABP) transcription factor has been shown in vitro to regulate the expression of the neuromuscular proteins utrophin, acetylcholine esterase, and acetylcholine receptor subunits δ and ε through the N-box promoter motif (5′-CCGGAA-3′), but its in vivo function remains unknown. A single point mutation within the N-box of the gene encoding the acetylcholine receptor ε subunit has been identified in several patients suffering from postsynaptic congenital myasthenic syndrome, implicating the GA-binding protein in neuromuscular function and disease. Since conventional gene targeting results in an embryonic-lethal phenotype, we used conditional targeting to investigate the role of GABPα in neuromuscular junction and skeletal muscle development. The diaphragm and soleus muscles from mutant mice display alterations in morphology and distribution of acetylcholine receptor clusters at the neuromuscular junction and neurotransmission properties consistent with reduced receptor function. Furthermore, we confirmed decreased expression of the acetylcholine receptor ε subunit and increased expression of the γ subunit in skeletal muscle tissues. Therefore, the GABP transcription factor aids in the structural formation and function of neuromuscular junctions by regulating the expression of postsynaptic genes.

Congenital myasthenic syndrome (CMS), is a heterogeneous disorder of neuromuscular transmission that occurs at a frequency of <1/500,000 people (42). CMS can be classified as presynaptic (i.e., choline acetyltransferase gene mutations), synaptic (i.e., acetylcholine esterase gene [*AChE*] mutations), or postsynaptic (i.e., acetylcholine receptor gene [*AChR*], or *Rapsyn*, mutations) in origin (14). All cases of CMS identified so far result in muscle weakness due to a lack of propagation of the endplate potential (13, 14). Understanding the molecular basis of CMS, and other neuromuscular diseases, may lead to the identification of potential therapies.

CMS is usually caused by missense mutations in the coding regions of neuromuscular junction (NMJ) proteins, such as ACh, AChE, or AChR subunits (30), or in postsynaptic AChR-associated proteins, such as Rapsyn (33). These mutations often result in structural changes of the AChR and altered affinity for ACh (34). In addition, a homozygous mutation in the N-box element (5′-CCGGAA-3′) of the *AChR*ε promoter results in a decreased number of AChRs and clinical symptoms of CMS (30, 32). This C→T transition in the mouse *AChR*ε promoter results in a 90% decrease in binding of the ETS transcription factor GA-binding protein (Gabp) (10).

The widely expressed ETS transcription factor Gabp regulates genes essential for the function of the NMJ, such as *AChR*δ and -ε (10, 23), *AChE* (3), and *Utrophin* (21), yet the molecular mechanism by which Gabp regulates NMJ-specific gene expression remains to be elucidated (39). In situ hybridization reveals that *Gabp*α mRNA is slightly enriched at NMJs relative to other muscle tissue, suggestive of synaptic function (40). The Gabp complex is composed of an α subunit (containing an ETS domain that binds a 5′-GGAA-3′ motif) and a β subunit (providing a nuclear localization signal and a transactivation domain) (25). GABP is phosphorylated at specific residues in both subunits in response to neuregulin-ErbB signaling, with receptor binding resulting in activation of the ERK and JNK serine-threonine kinases and, subsequently, the GABP complex, which then binds the N-box promoter elements of target genes (17).

Skeletal-muscle-specific, ETS dominant-negative mice exhibit muscles with small AChR patches and disorganized postsynaptic junctional folds (7). However, the ETS factor responsible for this phenotype was not identified. Our studies suggest that Gabpα is a likely candidate. Mice deficient in Gabpα die prior to implantation (35), thus restricting the use of these mice to prove a function for Gabp in AChR regulation in vivo. In this study, we examine the role of Gabp in skeletal muscle development and function by conditional targeting of *Gabp*α. These mice demonstrate defects in AChR assembly and synaptic transmission at the NMJ in skeletal muscle, highlighting the importance of Gabp in the development and function of postsynaptic structures at the NMJ.

* Corresponding author. Mailing address: Monash Institute of Medical Research, Monash Medical Centre, 246 Clayton Road, Clayton, Victoria 3168, Australia. Phone: 61 3 9594 7236. Fax: 61 3 9594 7211. E-mail: Paul.Hertzog@med.monash.edu.au.

† Present address: Genomics Institute of the Novartis Research Foundation, 10675 John Jay Hopkins Drive, San Diego, CA 92121.

‡ Present address: Merck Research Laboratories, Merck & Co., 126 East Lincoln Avenue, Rahway, NJ 07065.

§ Supplemental material for this article may be found at http://mcb.asm.org.

▽ Published ahead of print on 26 February 2007.

MATERIALS AND METHODS

Generation of a Gabpα targeting construct. A 3.2-kb BamHI-EcoRI genomic fragment, spanning introns 1 and 2 of Gabpα (bp 6662 to 9873 of GenBank accession no. GI:27960443), was inserted into the pBS KS$^+$ vector (Stratagene, La Jolla, CA) and constituted the 5′ and 3′ homologous sequences of the targeting construct. Exon 2 of *Gabpα* was removed by BclI digestion (bp 8212 to 8572 of GI:27960443) (35) and replaced with a 1.4-kb ApaI-NsiI fragment encompassing the floxed p*MCI-Neomycin* cassette. Finally, a 380-bp PCR product containing *Gabpα* exon 2 fused to a *loxP* site at its 5′ end (spanning bp 8220 to 8562 of GI:27960443) was inserted at a unique AatII site at the 5′ end of the *Neomycin* cassette. A negative selection marker, thymidine kinase, under the control of the *Herpes simplex virus* promoter, was introduced into the pBS KS(+) vector backbone at a unique XhoI site.

Generation of Gabpα floxed mice. Embryonic stem (ES) cells from mice of the SvJ129 background strain were electroporated with the *Gabpα* targeting construct (linearized at a SacII site within the vector backbone) and selected for 7 days using Geneticin at 15 mg/ml and ganciclovir at 2 μM, as previously described (24). Selected colonies were screened by Southern blotting and subsequently electroporated with PGK-Cre recombinase and PGK-puromycin constructs. Conditionally targeted (floxed) ES cell clones were screened by PCR following selection with 3 μg/ml puromycin for 2 days prior to injection into blastocysts from superovulated C57BL/6 female mice.

ES cell screening and generation of *Gabpα* floxed ES cells. Ten micrograms of genomic DNA was digested with 10 U BamHI overnight at 37°C prior to electrophoresis and Southern blot capillary transfer onto Gene Screen Plus nylon membrane (NEN, Boston, MA) according to the manufacturer's instructions. The membranes were hybridized as previously described (19), using a 977-bp SacII-SpeI probe within *Gabpα* intron 3 (bp 12695 to 13672 of GI:27960443) to identify a 7-kb wild-type and a 5-kb targeted fragment, respectively. ES cell clones were screened by PCR spanning intron 1 and intron 2 (primers G1f, 5′-GCTGTGCTTTGCCAGTGTTG-3′, and G1r, 5′-GACTAAGTGAGGACTATTGG-3′), generating 1.5-kb, 1.8-kb, and 1.9-kb fragments from the knockout, wild-type, and floxed alleles, respectively. The presence of the single *loxP* site immediately upstream of exon 2 was confirmed by multiplex PCR, using a common 5′ primer within intron 1 (G2f, 5′-CTCCTGAGGTCCCTGCTTTG-3′) and 3′ primers within exon 2 (G2r, 5′-GTCCCGTCGATCTCAATTTC-3′) and intron 2 (G1r, 5′-GACTAAGTGAGGACTATTGG-3′). This reaction generated 620-bp, 660-bp, and 740-bp fragments representing wild-type, floxed, and knockout *Gabpα* alleles, respectively.

Generation of Gabpα skeletal-muscle-specific knockout mice. *Gabpα* floxed mice were intercrossed with mice expressing the Cre recombinase transgene driven by the promoter of the human α-skeletal actin gene (described in reference 28) to generate heterozygous conditional-knockout mice of genotype *Gabpα*$^{F/+}$ *HSA*$^{cre/+}$. These mice (referred to here as +/−) were intercrossed to confirm a Mendelian ratio of allelic inheritance. Animals used for phenotypic analysis were generated from breeding homozygous floxed animals (*Gabpα*$^{F/F}$, referred to as wild type, or +/+, unless otherwise defined) with homozygous conditional mutant mice (*Gabpα*$^{F/F}$ *HSA*$^{cre/+}$, referred to as −/−). Genomic DNA was screened by PCR using 0.25 U *Taq* DNA Polymerase (Promega, Madison, WI), with annealing at 50°C and a 1-min extension time. Gabpα alleles were amplified with primers G2f, G2r, and G1r in reaction mixtures containing 2 mM $MgCl_2$. The *Cre* allele was detected by amplification with primers Cre-5′ (5′-CCGGTCGATGCAACGAGTGAT-3′) and Cre-3′ (5′-ACCAGAGTCATC CTTAGCGCC-3′) in reaction mixtures containing 1.5 mM $MgCl_2$. All experiments using mice were carried out in accordance with Australian federal regulations and approved by the Monash University ethics committee.

SDS-PAGE and Western blot immunodetection. Protein samples were prepared, electrophoresed through 8% nonreducing polyacrylamide gels, and transferred onto Immobilon-P membranes (Millipore, Bedford, MA) as previously described (37). Gabpα protein was detected by overnight incubation at 4°C with a rabbit polyclonal antibody generated against amino acids 40 to 147 (35) and subsequent incubation with 0.15 μg/ml goat anti-rabbit horseradish peroxidase-conjugated immunoglobulin G (IgG) (DAKO, Carpinteria, CA) for 1 h at room temperature prior to detection with SuperSignal West Pico Chemiluminescent Substrate (Pierce, Rockford, IL) and exposure to film (BioMax MR; Kodak, Rochester, NY). The film was developed in a Kodak X-OMAT 480 RA processor and scanned at 100 dots per inch using a Canon N1220U, and the intensities of bands were determined using FujiFilm MacBAS v2.5 software. Protein levels were quantified as a ratio to β-tubulin by detection with 0.05 μg/ml anti-β-tubulin mouse monoclonal antibody (Boehringer-Mannheim, Mannheim, Germany), followed by 0.3 μg/ml rabbit anti-mouse horseradish peroxidase-IgG (DAKO, Carpinteria, CA), and results from three animals per genotype were averaged across three duplicate blots.

Real-time RT-PCR analysis. The rapid acid guanidinium thiocyanate-phenol-chloroform method (5) was used for total-RNA preparation from mouse skeletal muscle tissues. Samples were treated with DNase I (Promega, Madison, WI), and ~10 μg of RNA was used as a template for first-strand cDNA synthesis using avian myeloblastosis virus reverse transcriptase (Promega, Madison, WI) and oligo(dT) primer according to the manufacturer's instructions. The relative expression levels of transcripts were determined using a Light Cycler (Roche, Mannheim, Germany) real-time reverse transcription (RT)-PCR machine (v3.5 software) according to the manufacturer's instructions and expressed as a ratio relative to β-actin. Specific primer sequences amplified the following RT-PCR products: AChRδ, bp 1021 to 1830 of GI:191609; AChRε, bp 3 to 258 of GI:2660742; utrophin, bp 10381 to 10603 of GI:1934962; Rapsyn, 827 to 918 bp of GI:53804; and β-actin, bp 344 to 446 of GI:49867.

Histology and fiber typing of skeletal muscle. Slides of transverse cryosections (16 μm) of skeletal muscle from 1-month-old mice were submerged in freshly made NADH staining solution (1 mg/ml 4-nitro blue tetrazolium [Sigma, Saint Louis, MO] and 0.8 mg/ml NADH [Sigma, Saint Louis, MO] dissolved in 0.2 M Tris-HCl, pH 7.4) and incubated at 37°C for 25 min in the dark. The slides were then rinsed in distilled water for 5 min prior to dehydration and mounting in histolene (Amber Scientific, Selmont, WA, Australia) and DePex (BDH, Poole, United Kingdom) solution. Images were taken with a Leica MPS60 digital camera on a Leica DMR microscope (Leica Instruments, Nussloch, Germany) at ×200 magnification.

Immunohistochemistry. Intact muscles were dissected and stained as previously described (22). For staining skeletal muscle tissue sections, dissected organs were rinsed in phosphate-buffered saline (PBS) and embedded directly into Tissue Tek optimal-cutting-temperature compound (OCT) (Sakura, Torrance, CA). OCT blocks were slowly frozen by placement into a plastic tray filled with 100% (vol/vol) isopentane resting on a bed of dry ice. The OCT tissue blocks were stored at −80°C. Prior to use, the tissue blocks were thawed to −20°C in the cryostat chamber for 30 min. Tissue was sectioned at 16 μm at −18°C using a Leica CM 3050 cryostat, and the tissue was collected onto Superfrost Plus (Menzel-Glaser, Braunschweig, Germany) glass slides. Prior to tissue staining, the mounted slides were thawed to room temperature and washed in PBS for 5 min to rid them of excess OCT compound.

AChR clusters were detected using Texas red-conjugated α-bungarotoxin (Molecular Probes, Eugene, OR) at 1 μg/ml. Nerves and synaptic terminals were localized in whole-mount samples by immunohistochemistry with rabbit sera raised against mouse 200-kDa neurofilament (8 μg/ml; Sigma, Saint Louis, MO) and human synaptophysin (1/50 neat sera; DAKO, Carpinteria, CA), and AChRδ and AChRγ proteins were detected in tissue sections with 2 μg/ml polyclonal rabbit antibodies sc-14000 and sc-13998 (Santa Cruz Biotechnology, Santa Cruz, CA). The antibodies were then visualized by use of 7.5 μg/ml Alexa 488-conjugated goat anti-rabbit IgG secondary antibody (Molecular Probes, Eugene, OR).

Stained fibers and tissue sections were imaged with a TCS NT digital camera on a DMRXE confocal microscope (Leica Instruments, Nussloch, Germany). NMJ areas of z-projected confocal images were calculated using ImageJ software. The values represent averages of six experiments, where for the floxed control, $n = 100$; for the mutant type 1, $n = 81$; and for the mutant type 2, $n = 26$.

^{125}I-labeled α-bungarotoxin staining. Intact soleus muscles were dissected from 3-month-old *Gabpα* conditional-knockout and littermate homozygous floxed mice and fixed in 2% (wt/vol) paraformaldehyde for 1 h at room temperature. Following three rinses (5 min each) in PBS, the muscles were teased into small fiber bundles and stained in a solution of 0.5-mg/ml acetylthiocholine iodide (Sigma, Saint Louis, MO) dissolved in 65 mM sodium acetate (pH 6.0), 1.5 mg/ml sodium citrate, 480 μg/ml cupric sulfate, and 170 μg/ml potassium ferricyanide for 30 min. Following three rinses (5 min each) in PBS, the synapse-rich regions were dissected away from the nonsynaptic regions of muscle fibers and then incubated in blocking solution (as described above) for 1 h at room temperature, followed by the addition of 10 nM [3-^{125}I]iodotyrosyl-α-bungarotoxin (Amersham Biosciences, Buckinghamshire, United Kingdom) for 4 h. The fibers were washed three times in 0.5% (vol/vol) Triton X-100 in PBS, for 15 min each time, prior to measurment of the radioactivity in a Packard Cobra 5005 gamma counter. Readings obtained for nonsynaptic regions were subtracted from those of synaptic regions for each muscle and were represented as an average of three experiments ($n = 18$). Means were compared using an unpaired Student's *t* test; *P* values of less than 0.05 were taken to be statistically significant.

Neuromuscular electrophysiology. Diaphragm and soleus muscles were dissected from 3-month-old *Gabpα* conditional-knockout and littermate control homozygous floxed mice, prepared, and stimulated as previously described (22).

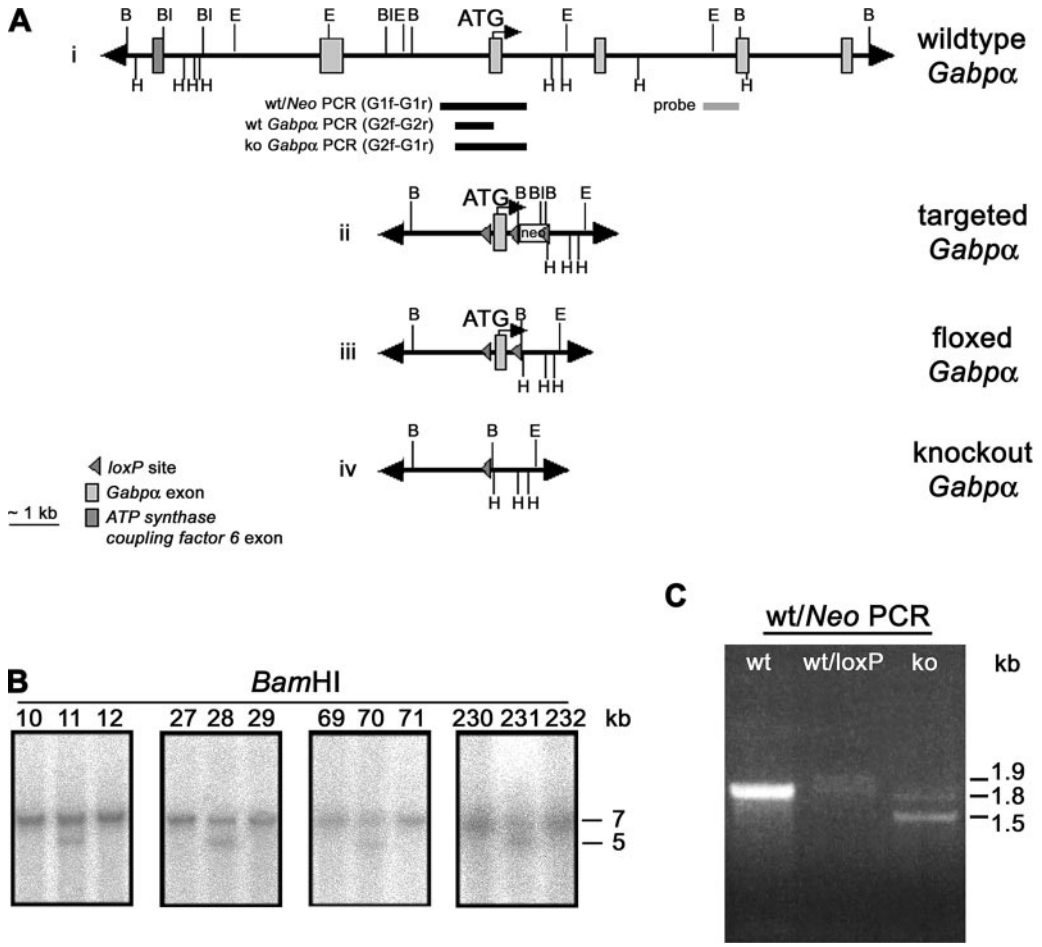

FIG. 1. Conditional targeting of the *Gabpα* locus. (A) Schematic of wild-type, targeted, floxed, and conditional-knockout *Gabpα* alleles. A floxed *Neomycin* (*neo*) cassette was inserted within intron 2, and a single *loxP* site immediately upstream of exon 2. The positions of the Southern blot probe, PCR primers and restriction sites for BamHI (B), BalI (Bl), EcoRI (E), and HindIII (H) are shown. (B) Southern blot analysis of genomic DNA from G418-resistant ES cells (clone numbers are shown), using a BamHI digest and an external intron 3 probe to detect 7-kb wild-type and 5-kb targeted fragments. (C) PCR screening of puromycin-resistant targeted ES cell clones following transient *Cre* transfection was performed with primers G1f and G1r, spanning *Gabpα* introns 1 and 2 flanking the site of insertion of the *neo* cassette, generating 1.8-kb wild-type (wt), 1.9-kb floxed (loxP), and 1.5-kb knockout (ko) allele products.

Extracellular recordings of the nerve terminal impulse (NTI), endplate currents (EPCs), and miniature endplate currents (MEPCs) were obtained using micropipettes (4-μm diameter). Focal extracellular recordings were obtained by adjusting the position of the electrode until both EPCs and MEPCs with rise times of less than 1 millisecond were detected. This method of recording was chosen because it measures the current underlying the intracellular potential changes if the electrode is close to the release site (2, 8, 16, 22); the electrode records the nerve terminal impulse as it passes along the nerve terminal, making it easy to check for action potential propagation failure as the cause for failure to release quanta (22), and the decay of the EPC gives an estimate of the closing times of many channels (11, 20). Care was taken to ensure that the frequencies of the EPCs and MEPCs did not change as the micropipette was lowered, since electrode pressure can give rise to an increase in the spontaneous frequency (16).

Once the NMJ was located, stimulation was halted for 5 min before recording MEPCs and EPCs to allow the terminals to replenish vesicle pools. Eight to 12 sites were selected for each muscle preparation, with at least 30 MEPCs and 100 to 200 stimulations recorded at each site. Four soleus muscles from each experimental group were examined. Extracellular recording sites were included for analysis if the frequencies of EPCs and MEPCs did not change due to electrode pressure and if at least one EPC was recorded during the first 10 stimuli. No correction for nonlinear summation was necessary, since all the EPCs recorded were less then 1 mV (27). The quantal content was calculated using either the methods of failures (if the proportion of failure to record an EPC was greater than 30%) (9) or by dividing the mean EPC amplitudes by the mean MEPC amplitudes (36). The rise times, decay times, and amplitudes and frequencies of evoked (EPC) and spontaneous (MEPC) releases were calculated and tabulated for each experimental group. The means were compared using an unpaired Student's *t* test; *P* values of less than 0.05 were taken to be statistically significant.

RESULTS

Generation of Gabpα conditional-knockout mice. Ubiquitous knockout Gabpα mice die early in embryogenesis (35). Therefore, to determine the in vivo role of Gabpα in skeletal muscle development and neuromuscular signaling, we generated mice lacking Gabpα specifically in skeletal muscle. To prevent the production of partial *Gabpα* transcripts, we targeted exon 2, the first coding exon, using the *Cre-loxP* system of bacteriophage P1 (41). A single *loxP* site was inserted immediately upstream of exon 2, and a floxed *Neomycin* cassette was cloned within intron 2 (Fig. 1A, ii). This construct was transfected into ES cells, and Southern blot analysis was used to identify four heterozygous targeted *Gabpα* ES clones (Fig. 1B). Transient transfection of Cre recombinase into targeted

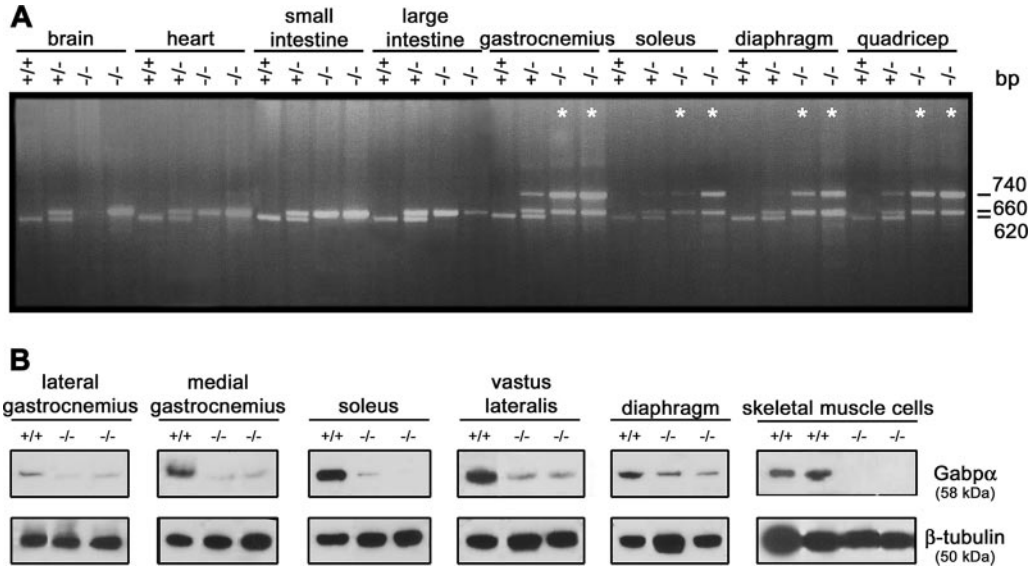

FIG. 2. Specific loss of Gabpα expression in skeletal muscle. (A) PCR screening of genomic DNA extracted from organs of wild-type (+/+), heterozygous (+/−), and homozygous knockout (−/−) mice. A common 5′ primer within intron 1 (G2f) and 3′ primers within exon 2 (G2r) and intron 2 (G1r) generated products of 620 bp, 660 bp, and 740 bp, representing wild-type, floxed, and knockout alleles, respectively. The knockout is represented by an asterisk in each case where no wild-type allele was detectable. (B) Western blot analysis of Gabpα (58-kDa) and β-tubulin (50-kDa) protein levels in skeletal muscle tissues and primary skeletal muscle cell cultures from *Gabpα* skeletal-muscle-specific knockout mice (−/−) relative to homozygous floxed (+/+) littermates. Severely reduced Gabpα protein levels were observed in whole muscle tissue lysates of Gabpα mutant mice and complete loss of Gabpα protein expression in *Gabpα* mutant primary skeletal muscle cells derived from mice at postnatal days 2 and 3.

clones 28 and 70 removed the *Neomycin* cassette to yield heterozygous floxed *Gabpα* (+/*loxP*) (Fig. 1A, iii). These clones were identified by PCR spanning introns 1 and 2 (Fig. 1C). ES cell clones containing the floxed *Gabpα* allele were injected into mouse blastocysts to yield chimeric mice. Seven lines that transmitted the floxed *Gabpα* allele were identified. All subsequent generations of mice were genotyped using a multiplex PCR, whereby the presence or absence of *Gabpα* exon 2 and the single remaining *loxP* site within intron 1 were confirmed by PCR amplification with primers spanning intron 1 and either exon 2 (wild-type and floxed alleles) or intron 2 (knockout allele) (see Fig. S1 in the supplemental material).

Conditional loss of Gabpα expression in skeletal muscle was achieved by intercrossing mice carrying floxed *Gabpα* and human alpha skeletal actin (*hαSA*)-*Cre* alleles (Fig. 1A, iv). The *hαSA-Cre* mouse line expresses Cre recombinase specifically in skeletal muscle, from embryonic day 9.5 (28). Amplification of a 797-bp PCR product from the *hαSA-Cre* allele confirmed the presence of the transgene (see Fig. S1 in the supplemental material). The resultant litters from these intercrosses gave the expected frequency of each genotype according to Mendelian inheritance ($n = 410$).

Loss of Gabpα expression specifically in skeletal muscle. We characterized genomic DNA from various tissues and showed that a 740-bp PCR product representing the *Gabpα* knockout allele is detected only in skeletal muscle tissues of heterozygous and homozygous conditional-knockout mice (Fig. 2A), consistent with specific expression of Cre recombinase. The wild-type allele is represented by a 620-bp band in all tissues, except skeletal muscle of homozygous mutants, and the floxed *Gabpα* allele is represented by a 660-bp band (Fig. 2A). The presence of the floxed PCR product in skeletal muscle of homozygous mutants indicates the presence of nonmuscle cell types in whole-tissue lysates (Fig. 2A).

We then examined lateral and medial gastrocnemius, soleus, vastus lateralis, and diaphragm muscles for Gabpα protein expression in floxed, heterozygous, and homozygous skeletal muscle-specific knockout mice by Western blotting (Fig. 2B shows a representative blot). Gabpα protein levels, quantified relative to β-tubulin (see Fig. S2 in the supplemental material), demonstrated a significant reduction ($P < 0.05$; $n = 3$; Student two-tailed t test) in Gabpα expression in all muscles examined from homozygous *Gabpα* skeletal muscle-specific knockout mice, ranging from 25 to 55% of normal levels in the soleus and diaphragm, respectively. Gabpα expression levels in heterozygous mice also varied in a tissue-specific manner, from 20 to 85% of normal levels in the medial gastrocnemius and diaphragm, respectively (data not shown). The residual Gabpα protein detected in muscle tissues of *Gabpα* mutant mice was likely due to heterogeneous Cre expression in multinucleated fibers and/or the presence of nonskeletal muscle cell types in these tissues. Immunohistochemistry of single skeletal muscle fibers from adult *Gabpα* mutant mice demonstrated variable Cre expression (data not shown), and Western blot analysis of Gabpα expression in primary skeletal muscle cultures isolated from 2- to 3-day-old pups revealed undetectable protein levels in animals homozygous for the *Gabpα* mutation (Fig. 2B).

We also examined protein extracts for the presence of altered Gabpα proteins in knockout muscle in order to confirm that conditional targeting and deletion of *Gabpα* exon 2 does not result in C-terminally truncated proteins that may produce hypomorphic or dominant-negative functions of Gabp. We

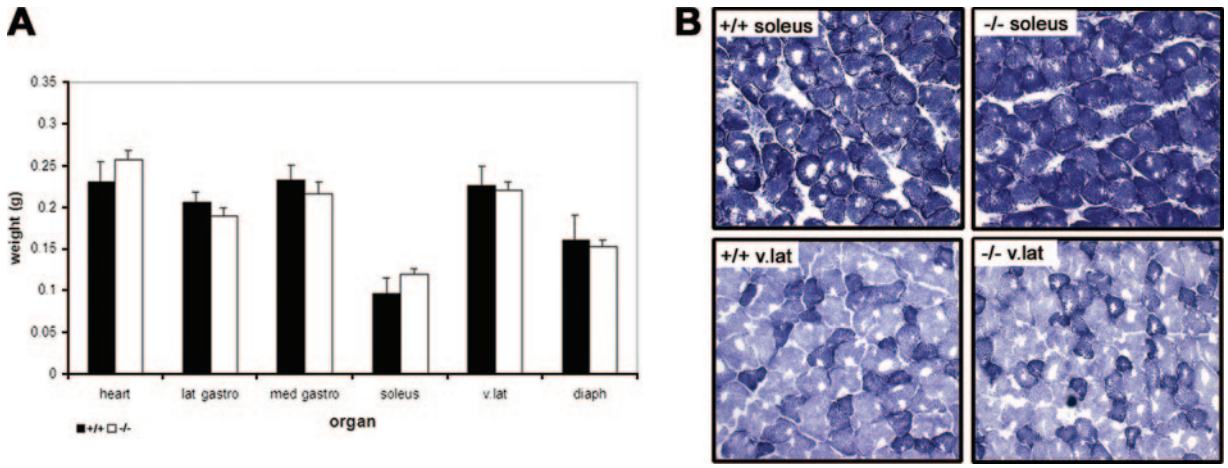

FIG. 3. (A) Organ weights of heart and various skeletal muscle tissues (lateral gastrocnemius, medial gastrocnemius, soleus, vastus lateralis, and diaphragm) showed no statistical difference between samples from 1-month-old homozygous floxed (+/+) and *Gabp*α skeletal-muscle-specific knockout (−/−) mice. (B) NADH staining of transverse cryosections from 1-month-old homozygous floxed (+/+) and *Gabp*α skeletal-muscle-specific knockout (−/−) mice showing no significant difference in fiber size or tissue integrity between the two genotypes. Type I, IIb, and IIa fibers are shown by dark, light, and intermediate staining, respectively. The images were taken at ×200 magnification.

performed Western analysis with a monoclonal antibody generated against the C terminus of Gabpα (a kind gift of S. Burden, The Skirball Institute). This antibody detected a protein product of a size similar to that of our N-terminal antibody, and there were no smaller (potentially truncated) proteins detected in knockout muscle (data not shown). Given that the ATP synthase coupling factor 6 gene is proximal to *Gabp*α and the two genes are known to share some common regulatory elements (4), we examined whether conditional targeting of *Gabp*α resulted in disruption of and or aberrant expression of ATP synthase coupling factor 6. Real-time RT-PCR analysis revealed no difference in expression levels between wild-type, homozygous floxed, and homozygous knockout muscles (data not shown).

Phenotype analysis of skeletal-muscle-specific *Gabp*α knockout mice. Gabpα does not appear to be essential for the growth and development of skeletal muscle, as the body weights of homozygous floxed and homozygous *Gabp*α conditional-knockout mice did not differ from 1 to 6 months of age, and histological analysis of muscle tissue from 1- to 6-month-old animals by hematoxylin and eosin staining and DAPI (4′,6′-diamidino-2-phenylindole) staining showed no difference in the proportions of centronucleated regenerating fibers (data not shown). Skeletal muscle tissues were weighed at 3 months of age, and no significant difference was found between homozygous floxed and homozygous *Gabp*α conditional-knockout mice (Fig. 3A). In addition, NADH staining of fresh transverse muscle sections revealed no atrophy of skeletal muscle fibers in *Gabp*α mutant mice (Fig. 3B). Footprint analysis comparing the regularity of gait of *Gabp*α skeletal-muscle-specific knockout and homozygous floxed mice at 1, 3, and 6 months of age also revealed no differences (data not shown). The lack of an overt phenotype in skeletal muscle of *Gabp*α mutant mice may be due to the high safety factor of neurotransmission found in mice in comparison to humans (26).

Gabpα is necessary for normal NMJ formation. AChR distribution was analyzed (by staining with a Texas red conjugate of α-bungarotoxin) in lateral and medial gastrocnemius, soleus, and vastus lateralis muscles from homozygous floxed and homozygous *Gabp*α mutant mice at 1, 3, and 6 months of age, and no difference was apparent (data not shown), indicating that Gabpα is not essential for the formation of postsynaptic AChR clusters. We examined the gross morphology of the NMJ by whole-mount staining for pre- and postsynaptic elements, using antibodies to synaptophysin-neurofilament and α-bungarotoxin, respectively. Individual muscle fibers were obtained from soleus muscles from homozygous floxed and *Gabp*α mutant mice at 3 months of age. As shown by the representative images in Fig. 4A, the morphologies of NMJs in *Gabp*α mutant mice were classified into two groups. First, 76% of soleus NMJs of homozygous *Gabp*α skeletal-muscle-specific knockout mice showed less branching than those of homozygous floxed *Gabp*α controls but appeared relatively normal and were classified as type 1. The remaining 24% of soleus NMJs showed a single ring structure and were classified as type 2. Similar proportions of the two classes of NMJs were observed in diaphragm and sternomastoid muscles (data not shown), but the soleus muscle was chosen for all quantification because of the relatively large size of the NMJs.

AChR-positive areas, as determined by α-bungarotoxin staining, were quantified for both type 1 and type 2 mutant NMJs and then expressed as percentages of the total NMJ area (Fig. 4B). Type 1 knockout NMJs of the soleus muscle were significantly increased in both the area occupied by AChRs and the total area of the NMJ ($P = 0.0008$ and $P = 0.0024$; $n = 81$; Student two-tailed t test) (Fig. 4C, center column). However, the percentage of the area occupied by AChRs was unchanged relative to the controls. By contrast, type 2 knockout NMJs were of equal area relative to control mice yet showed a significant decrease in the percentage of the area occupied by AChRs ($P = 0.034$; $n = 26$; Student two-tailed t test) (Fig. 4D, right column). The increased area occupied by AChRs observed in 76% of *Gabp*α mutant NMJs (type 1 morphology) corresponded to an observed 1.8-fold increase in the number

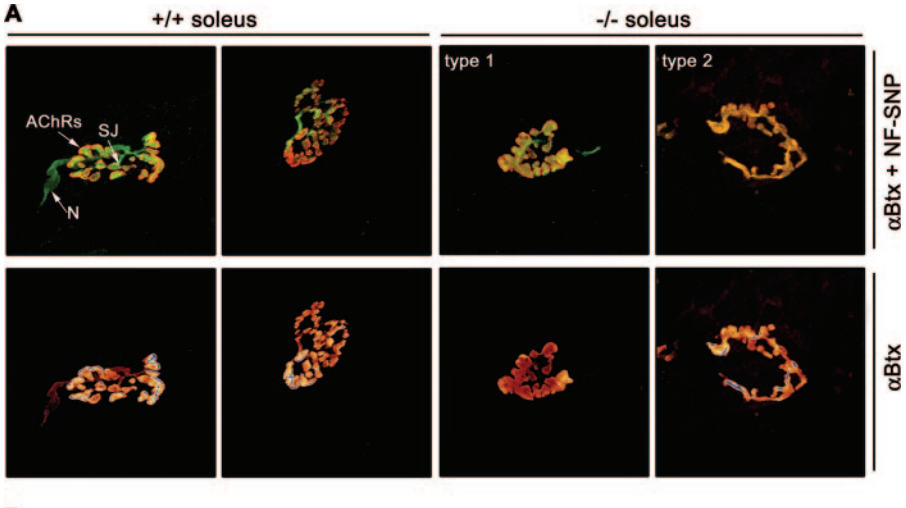

C

	+/+	-/- type 1 (76%)	-/- type 2 (24%)
AChR Positive Area	11413 +/- 1731	15695 +/- 2118 *	12921 +/- 2004
Total NMJ Area	16318 +/- 2868	22592 +/- 3457 *	19968 +/- 3545
% AChR/Total Area	73 +/- 2	72 +/- 2	67 +/- 2 *

FIG. 4. NMJ morphology in soleus muscles of *Gabpα* conditional-knockout mice. (A) Whole-mount immunostaining of single muscle fibers from 3-month-old control homozygous floxed (+/+) and homozygous *Gabpα* skeletal-muscle-specific knockout (−/−) mice. NMJ shape is revealed by AChR staining with Texas red-conjugated α-bungarotoxin (αBtx). Nerves and synaptic junctions were stained with a cocktail of fluorescein isothiocyanate-conjugated antibodies against neurofilament and synaptophysin (NF-SNP). The relative positions of nerves (N), synaptic junctions (SJ), and AChRs are indicated in the top left panel. NMJs of −/− mice are classified as showing less branching than those of control mice (type 1) or single ring structures (type 2). All images are at ×1,000 magnification. (B) Schematic representation of how the AChR-positive and total NMJ areas were defined, using the freehand tool in Image J image analysis software. The AChR-positive area was taken to be that area stained with α-bungarotoxin (btx) at the terminus of the synaptic nerve. The total NMJ area was taken to encompass the entire AChR-positive area, leaving no internal space between the outermost branches. (C) Quantified synaptic areas occupied by AChRs, total NMJ areas (expressed in arbitrary units ± standard errors of the mean), and percentage of the area occupied by AChRs of NMJs of 3-month-old homozygous floxed (+/+) and homozygous *Gabpα* skeletal-muscle-specific knockout (−/−) mice. *, $P < 0.05$ (Student's two-tailed *t* test). Types 1 and 2 are the two morphological types of NMJs observed in *Gabpα* mutant animals at a frequency of 76% and 24%, respectively.

of AChRs found in the synaptic region of ^{125}I-labeled α-bungarotoxin-stained soleus muscles from 3-month-old *Gabpα* knockout mice in comparison to control littermates (12,559 versus 6,939 counts; $P = 0.013$; $n = 9$) (see Fig. S3 in the supplemental material).

No difference in the distributions and appearance of mitochondria, synaptic vesicles, or postsynaptic junctional folds was detected at the NMJs of 3-month-old *Gabpα* skeletal-muscle-specific knockout mice and homozygous floxed controls, as determined by electron microscopic examination of soleus and diaphragm muscles (data not shown).

Neuromuscular spontaneous and evoked transmitter release is reduced in *Gabpα* mutant mice. Given the alterations in morphology and number of postsynaptic AChRs of NMJs from *Gabpα* skeletal-muscle-specific knockout mice, we examined NMJ physiology in these mice. We measured evoked EPCs, MEPCs, and the NTI at NMJs of diaphragm and soleus muscles from *Gabpα* mutant and homozygous floxed littermate control mice at 3 months of age. These parameters were used to calculate the mean quantal content, a measure of the average evoked release of acetylcholine from motor nerve terminals. The NTI was recorded in every extracellular recording, although EPCs were highly intermittent in both knockout and control NMJs and no intermittence in the NTI was observed throughout the recordings (Fig. 5A and E). This suggested that the decrease in the evoked transmitter release and associated

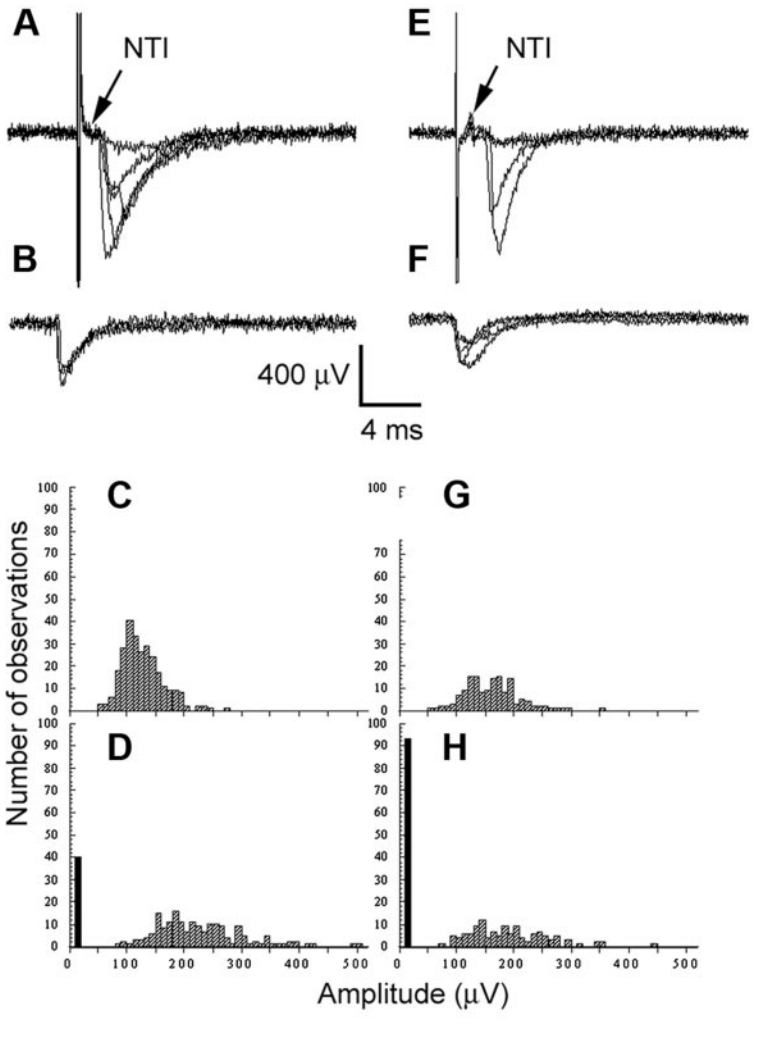

I

Soleus		
	+/+	-/-
No. of mice	4	4
No. of sites recorded	12	12
MEPC:		
Amplitude (μV)	277.44 ± 32.41	171.15 ± 25.98*
Rise time (ms)	0.70 ± 0.02	0.67 ± 0.02
Decay constant (ms)	2.83 ± 0.33	8.27 ± 2.25*
EPC:		
Amplitude (μV)	418.21 ± 68.00	167.16 ± 15.08**
Rise time (ms)	1.01 ± 0.10	0.99 ± 0.05
Mean quantal content	1.04 ± 0.12	0.51 ± 0.15**
Diaphragm		
	+/+	-/-
No. of mice	4	4
No. of sites recorded	11	13
MEPC:		
Amplitude (μV)	187.70 ± 31.62	256.60 ± 36.74
Rise time (ms)	0.72 ± 0.02	0.90 ± 0.04***
Decay constant (ms)	3.48 ± 0.39	8.36 ± 1.61**
EPC:		
Amplitude (μV)	342.88 ± 66.00	268.47 ± 34.20
Rise time (ms)	1.42 ± 0.1	1.15 ± 0.07*
Mean quantal content	1.42 ± 0.16	0.70 ± 0.13**

J

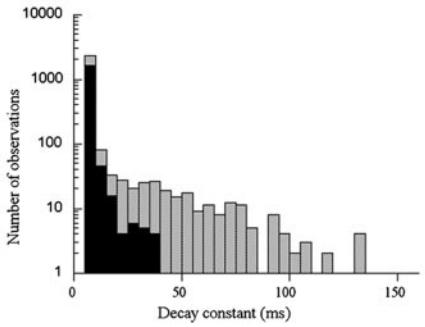

FIG. 5. Extracellular recordings from NMJs of homozygous floxed control (A to D) and *Gabp*α conditional knockout mice (E to H). Panels A and E show examples of evoked EPCs. Panels B and F show examples of MEPCs. In panels A, B, E, and F, five consecutive traces are superimposed. Note the invariable presence of the NTI in both control (A) and mutant (E) recordings. Frequency amplitude histograms of MEPCs (C and G) and evoked (D and H) amplitudes are shown. The histograms shown in panels C and D were constructed from a single recording site, as were the histograms shown in panels G and H. The distributions of MEPC amplitudes were similar in both control and *Gabp*α conditional-knockout mice. EPCs were skewed toward higher amplitudes in control mice, and the number of failures (black bars) was higher at NMJs from *Gabp*α mutant mice (H) compared to controls (D). (I) Comparison of biophysical properties of 3-month-old homozygous floxed *Gabp*α control (+/+) and *Gabp*α conditional-knockout (−/−) mice. *, $P < 0.05$; **, $P < 0.01$; ***, $P < 0.001$ (Student's two-tailed *t* tests). (J) Representation of MEPC decay rate constants from NMJs of *Gabp*α conditional-knockout (hatched bars) and homozygous floxed (black bars) mice. The histograms were constructed from a single recording site taken from either mutant or control soleus muscle. The decay rate constants for control MEPCs varied from 10 ms to 35 ms. In contrast, the decay rate for *Gabp*α mutant mice varied from 10 ms to 130 ms. This resulted in a significantly longer mean in decay rates at NMJs of *Gabp*α conditional-knockout mice than in control animals.

increased failure rate of stimuli to evoke transmitter release in *Gabp*α mutant terminals were not due to failure of the action potential to invade the nerve terminal (Fig. 5) but rather a failure of depolarization-secretion coupling.

The amplitudes of both the MEPCs and EPCs were significantly reduced at soleus NMJs from *Gabp*α knockout mice compared to control mice (Fig. 5I). The mean amplitudes for MEPCs were 171.15 ± 25.98 μV for knockout mice and 277.44 ± 32.41 μV for controls ($P = 0.018$; $n = 12$; Student's paired *t* test). Furthermore, the mean EPC amplitudes appeared to be no greater than MEPC mean amplitudes at NMJs from *Gabp*α knockout NMJs (167.16 ± 15.08 μV) (Fig. 5I). By constructing amplitude frequency histograms of MEPCs and EPCs, we were able to estimate quantal contents. The quantal content was significantly lower in the mutant nerve terminals from soleus and diaphragm muscles (Fig. 5I). These results indicated that both presynaptic and postsynaptic abnormalities had occurred at NMJs from *Gabp*α conditional-knockout mice, culminating in the observed drop in the mean quantal content.

NMJ decay constants are significantly longer in *Gabp*α mutant mice. Gabp is a key member of the ARIA/Heregulin/

Neuregulin-ErbB signal transduction pathway (17). This pathway drives expression of the postsynaptic *AChR*ε subunit gene, thus triggering the change of composition of AChRs from fetal ($\alpha\beta_2\delta\gamma$) to adult ($\alpha\beta_2\delta\varepsilon$) by the end of postnatal week 1, allowing longer AChR channel opening times when ACh binds to its receptor. We therefore examined the decay constants (a measure of the channel opening time) at soleus and diaphragm NMJs from 3-month-old *Gabp*α skeletal-muscle-specific knockout and homozygous floxed littermate control mice and observed that the decay constants at NMJs from *Gabp*α mutant mice were significantly longer than those of control mice (Fig. 5I and J). The mean decay constant of MEPCs for *Gabp*α mutant soleus NMJs was 8.27 ± 2.25 ms, compared to 2.83 ± 0.33 ms for control NMJs ($P = 0.026$; $n = 12$; Student's paired *t* test). Similar differences were observed for diaphragm *Gabp*α knockout NMJs (Fig. 5I). Frequency histograms from individual recording sites typically showed a highly positive skew of the decay constants ranging out to 100 to 150 ms in duration at soleus and diaphragm *Gabp*α mutant NMJs compared to 30 to 40 ms for control NMJs (Fig. 5J). The increase in the MEPC decay constant is consistent with a failure to express sufficient levels of AChRε, a likely consequence of *Gabp*α gene inactivation in skeletal muscles of *Gabp*α mutant mice.

The alterations in electrophysiology of *Gabp*α mutant NMJs did not, however, result in any significant change in skeletal muscle fatigability (at 1 year of age) or in strength (from 1 to 6 months of age), as determined by rotarod and wire grip tests, respectively (data not shown).

Altered AChR expression levels in skeletal muscle of *Gabp*α mutant mice. In order to explain the underlying cause of changes in NMJ structure and function in *Gabp*α mutant mice, we examined the expression levels of Gabp target genes. Individual diaphragm muscles from four floxed mice and four homozygous mutant mice at 3 months of age were studied, using real-time RT-PCR to quantify the levels of *AChR*δ, *AChR*ε, and *Utrophin* (Fig. 6A). *AChR*ε expression was decreased 10-fold ($P = 0.0000013$; $n = 12$; Student two-tailed *t* test) in *Gabp*α mutant diaphragms. Although the mean expression level of *AChR*δ was 50% of normal in mutant diaphragms, the high degree of variability between floxed animals of mixed-strain background obscured the statistical significance of these data. Interestingly, analysis of cDNA from soleus muscles of the same animals showed no significant difference between genotypes (data not shown). However, a large decrease in the mean expression level of *AChR*δ was again masked by a large variation in floxed controls. *Utrophin* levels were unaltered in skeletal muscle of *Gabp*α knockout mice compared to their floxed littermates (Fig. 6A), suggesting Gabpα is not required for transcriptional activation of *Utrophin*, at least in these tissues, and immunostaining of soleus muscle fibers showed no change in utrophin protein expression between genotypes (data not shown).

These real-time RT-PCR data do, however, validate AChR subunits as target genes regulated by Gabp. Furthermore, immunostaining of medial gastrocnemius tissue sections from 3-month-old mice with antibodies specific for AChRδ and AChRγ expression (Santa Cruz Biotechnology, Santa Cruz, CA) confirmed that expression of AChRδ protein was unchanged in the *Gabp*α mutant compared to homozygous floxed controls (Fig. 6B). However, protein levels of AChRγ were upregulated in the *Gabp*α skeletal-muscle-specific knockout animal (Fig. 6B). The fetal AChRγ subunit is normally replaced by the adult AChRε subunit within the first two postnatal weeks in mice (29), resulting in a change in ion channel properties. This increase in AChRγ protein expression correlates well with the observed decrease in *AChR*ε transcript levels and explains the increased decay constants of MEPCs of *Gabp*α mutant mice compared to those of littermate controls. AChR expression may also be regulated by the basic helix-loop-helix factors myogenin and MyoD. However, we did not observe an up-regulation of these proteins (data not shown), indicating that altered expression of AChR subunits is due directly to loss of Gabpα expression.

DISCUSSION

We generated *Gabp*α skeletal-muscle-specific knockout mice that demonstrated reduced levels of the target gene *AChR*ε in the diaphragm, altered distribution of AChRs at the NMJ, and abnormal neurotransmission properties, resulting from a compensatory increase in AChRγ expression. This model demonstrates an important role for Gabpα in the structure and function of neuromuscular synapses.

We showed that expression of the Gabp target gene *AChR*ε is decreased in the diaphragms of *Gabp*α knockout mice. A trend toward reduced mRNA levels of *AChR*δ was observed, and no change in *Utrophin* expression levels was apparent. This indicates that other transcription factors, including other ETS proteins, expressed in skeletal muscle cells may, to some degree, compensate for loss of Gabpα expression. This is supported by reduced levels of *Utrophin*, *AChR*ε, and *AChE* in the vastus lateralis of mice expressing a dominant-negative ETS (comprised of the ETS DNA binding domain) protein in skeletal muscle (7). In addition, although our data showing decreased *AChR*ε expression in the absence of Gabp function agree with those of Briguet and Ruegg (1), an impairment in AChR clustering was also observed following in vivo injection of a Gabpβ dominant-negative construct into rat soleus muscle fibers (1), suggesting that the milder phenotype observed in this study may be partly explained by the ability of Gabpβ to partner with another transcription factor. Interestingly, expression of a dominant-negative ETS protein results in transgenic mice with an altered AChR morphology at the NMJ (7). These data clearly imply a role of skeletal-muscle-expressed ETS factors in NMJ function, and the findings are strikingly similar, although more severe, than those described here for *Gabp*α skeletal muscle knockout mice.

The physiological effect of loss of Gabpα expression upon neuromuscular transmission resembles that of mice lacking the ErbB2 and ErbB4 neuregulin receptors in skeletal muscle (15). Like skeletal-muscle-specific *Gabp*α knockout mice, adult mice lacking neuregulin signaling specifically in skeletal muscle have decreased MEPC amplitudes and low MEPC decay rates (15). This further validates Gabp as a key effecter of the neuregulin-ErbB signaling pathway and emphasizes a specific function of Gabp at the NMJ that cannot be compensated for by other proteins.

Previous mutation studies have identified the N-box (ETS site) as a critical element for synapse-specific expression of both *AChR*δ (18, 23) and -ε (10). While we have shown de-

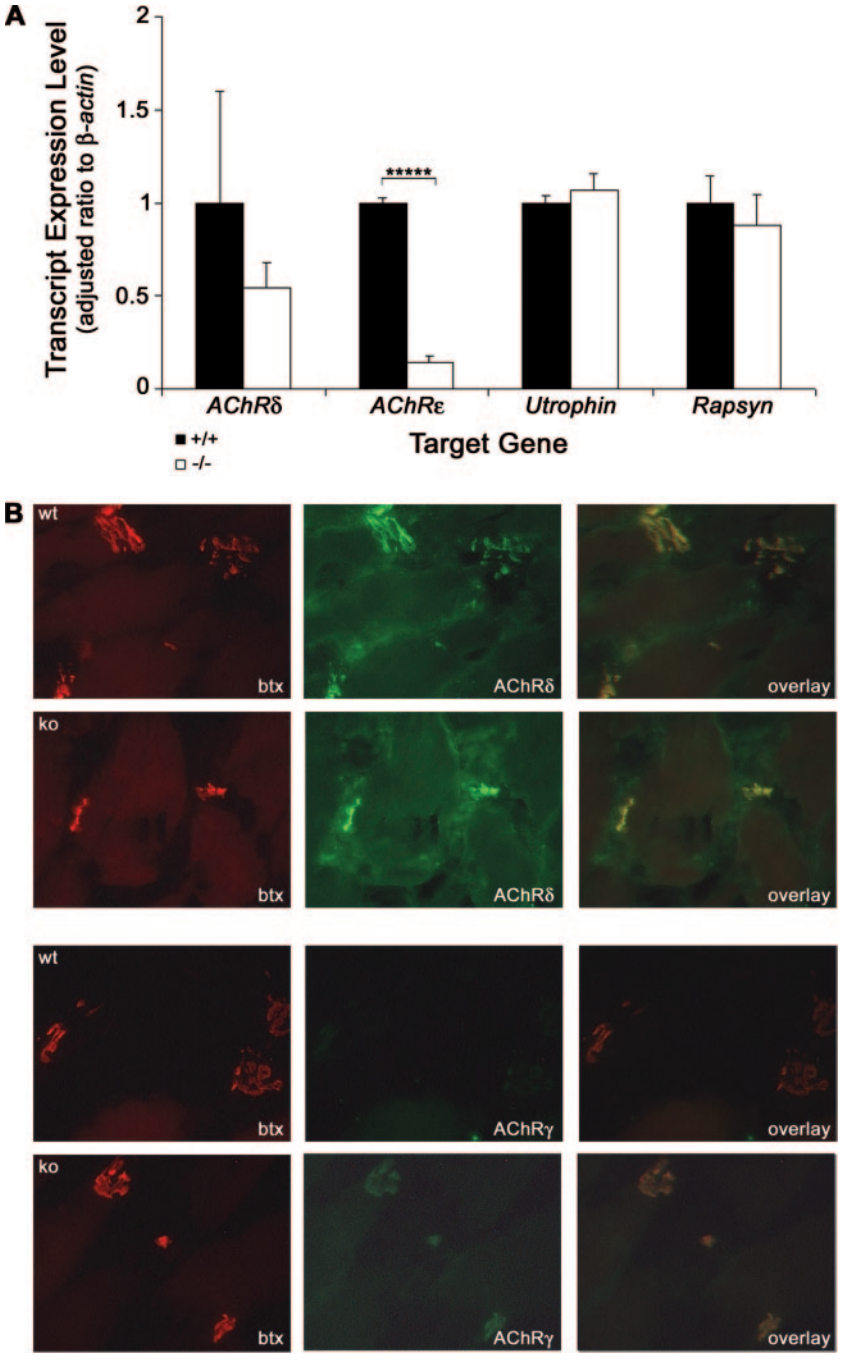

FIG. 6. Expression of Gabp target genes in *Gabp*α conditional-knockout mice. (A) Real-time RT-PCR analysis of transcript levels of Gabp target genes, using cDNA from diaphragm muscles of four 3-month-old homozygous floxed (+/+) and homozygous *Gabp*α skeletal muscle-specific knockout (−/−) mice. The expression levels of each transcript are expressed as a ratio to β-actin. The ratios were adjusted so those of floxed mice were 1. The error bars represent standard errors of the mean. *****, $P < 0.000005$; $n = 12$ (two-tailed Student's *t* test). Levels of *Rapsyn* were measured as a negative control, as it is not a Gabp gene target. (B) Immunostaining of transverse cryosections from 3-month-old homozygous floxed (+/+) and *Gabp*α skeletal-muscle-specific knockout (−/−) mice with Texas red-conjugated α-bungarotoxin (btx) and antibodies recognizing AChRδ or AChRγ showing colocalization and increased expression of AChRγ in *Gabp*α mutant mice. The images were taken at ×400 magnification.

creased *AChR*ε gene expression, this drop had no effect upon postsynaptic localization and clustering of AChRs in muscles of *Gabp*α skeletal-muscle-specific knockout mice, suggesting that Gabpα is not essential for the formation of postsynaptic AChRs. However, loss of Gabpα expression does result in altered NMJ morphology in knockout muscles. In agreement with the phenotype of mice expressing a dominant-negative ETS protein in skeletal muscle (7), we observed that type 2

NMJs of *Gabpα*$^{-/-}$ soleus muscles showed a single ring structure and a significant decrease in the percentage of the area occupied by AChRs, with the remaining type 1 NMJs showing less branching than those of homozygous floxed *Gabpα* controls.

Type 1 NMJs of *Gabpα* conditional-knockout mice had an increased area compared to those of wild-type mice, but the percentage of the area occupied by AChRs remained unchanged. This corresponds to the observed increase in the total number of AChRs found in the synaptic region of soleus muscle tissues from *Gabpα* conditional-knockout mice. The increase in AChR protein expression in *Gabpα* mutant mice may be a secondary effect of loss of Gabpα expression if the muscle is responding to ineffective innervation. In addition, the multinucleated nature of skeletal muscle cells means that variable Cre splicing efficiency of *Gabpα* in myonuclei along a muscle fiber may result in altered neuromuscular transmission without resulting in an overall decrease in AChR protein expression.

Together with the lower MEPC and EPC mean amplitudes at *Gabpα* mutant soleus NMJs, these data suggest that although compensatory mechanisms may allow AChR protein expression at the NMJ in the absence of Gabpα, altered distribution of these receptor molecules within an NMJ results in impaired neuromuscular signaling. Specifically, we observed reduced EPC and MEPC amplitudes, leading to a 50% drop in the mean quantal content in NMJs of *Gabpα* mutant mice. The longer decay times of EPCs at NMJs of the *Gabpα* mutant animals is explained by the observed upregulation of AChRγ expression in an attempt to compensate for the loss of the AChRε protein at the NMJs of conditional-knockout mice. Upregulation of AChRγ expression has been observed in mice lacking AChRε (43) and some humans suffering from CMS (12), resulting in an increase in the channel opening time (and current decay time) and a decrease in the amplitude of endplate potentials. However, the high safety factor of neurotransmission in mice (26), together with the increased total number of AChRs observed in synaptic regions of soleus muscles lacking Gabpα expression, suggests that sufficient AChRε protein is made in the absence of Gabpα expression to allow overtly normal skeletal muscle function. The high safety factor is clearly demonstrated by mice lacking the neuromuscular structural protein utrophin, which are healthy and show no signs of muscle weakness despite postsynaptic abnormalities, such as low numbers of AChRs and fewer junctional folds (6).

It would be of interest in the future to study mice of up to 2 years of age for any signs of deterioration, as the human α-skeletal actin gene promoter used to drive Cre expression in this study was previously shown to allow high levels of regeneration of muscle fibers through residual gene expression in satellite cells (31). However, no histological signs of such compensation were visible up to 6 months of age, and preliminary rotarod and grip analyses of *Gabpα* mutant mice up to 1 year old showed no loss of coordination, balance, or muscle strength. Studies are also under way to better understand the in vivo role of Gabpα in the regulation of nuclear encoded genes of mitochondrial function, such as subunits of cytochrome *c* oxidase. Early embryonic lethality of complete *Gabpα* knockout mice (35), and our preliminary results showing decreased levels of mitochondrial transcription factor A and altered fiber type proportions in *Gabpα* skeletal-muscle-specific mutants (data not shown), support the idea put forth in numerous in vitro studies; Gabpα (also known as nuclear respiratory factor 2) is a key regulator of cellular metabolism (38).

The loss of Gabpα expression in skeletal muscle results in irregular NMJ morphology and decreased EPC amplitude, mean quantal content, and decay time, indicating that the Gabp complex is necessary for the development of functional NMJs within skeletal muscle fibers. Interestingly, disruption of Gabp function by mutation of the N box of the target gene *AChRε* results in postsynaptic muscular disease. Therefore, disruption of Gabpα expression could be an underlying cause of human diseases, such as CMS.

ACKNOWLEDGMENTS

We are very grateful to the Monash Medical Centre animal house staff, E. De Luca, S. Tsao, D. Finkelstein, I. Harper, T. Wilson, and L. Mittaz Crettol for their technical assistance and helpful comments throughout this work. We thank Judith Melki and Edna Hardeman for providing the *hαSA-Cre* mouse line, Klaus Rajewsky for kindly providing the floxed p*MCI-Neomycin* cassette, Steve Burden for providing Gabpα-specific antisera, and Michael Liang for technical support.

This work was supported by grants from the Australian National Health and Medical Research Council (S.R., P.G.N., and P.J.H.).

REFERENCES

1. **Briguet, A., and M. A. Ruegg.** 2000. The ETS transcription factor GABP is required for postsynaptic differentiation *in vivo*. J. Neurosci. **20:**5989–5996.
2. **Brock, J. A., and T. C. Cunnane.** 1987. Relationship between the nerve action potential and transmitter release from sympathetic postganglionic nerve terminals. Nature **326:**605–607.
3. **Chan, R. Y. Y., C. Boudreau-Larivière, L. M. Angus, F. A. Mankal, and B. J. Jasmin.** 1999. An intronic enhancer containing an N-box motif is required for synapse- and tissue-specific expression of the acetylcholinesterase gene in skeletal muscle fibers. Neurobiology **96:**4627–4632.
4. **Chinenov, Y., C. Coombs, and M. E. Martin.** 2000. Isolation of a bi-directional promoter directing expression of the mouse GABPα and ATP synthase coupling factor 6 genes. Gene **261:**311–320.
5. **Chomczynski, P., and N. Sacchi.** 1987. Single-step method of RNA isolation by acid guanidinium thiocyanate-phenol-chloroform extraction. Anal. Biochem. **162:**156–159.
6. **Deconinck, A. E., A. C. Potter, J. M. Tinsley, S. J. Wood, R. Vater, C. Young, L. Metzinger, A. Vincent, C. R. Slater, and K. E. Davies.** 1997. Postsynaptic abnormalities at the neuromuscular junctions of utrophin-deficient mice. J. Cell Biol. **136:**883–894.
7. **de Kerchove d'Exaerde, A., J. Cartaud, A. Ravel-Chapuis, T. Seroz, F. Pasteau, L. M. Angus, B. J. Jasmin, J.-P. Changeux, and L. Schaeffer.** 2002. Expression of mutant Ets protein at the neuromuscular synapse causes alterations in morphology and gene expression. EMBO Rep. **3:**1075–1081.
8. **Del Castillo, J., and B. Katz.** 1956. Localization of active spots within the neuromuscular junction of the frog. J. Physiol. **132:**630–649.
9. **Del Castillo, J., and B. Katz.** 1954. Quantal components of the end-plate potential. J. Physiol. **124:**560–573.
10. **Duclert, A., N. Savatier, L. Schaeffer, and J.-P. Changeux.** 1996. Identification of an element crucial for the sub-synaptic expression of the acetylcholine receptor ε-subunit gene. J. Biol. Chem. **271:**17433–17438.
11. **Dudel, J., and M. Heckmann.** 2002. Quantal endplate currents from newborn to adult mice and the switch from embryonic to adult channel type. Neurosci. Lett. **326:**13–16.
12. **Engel, A. G., K. Ohno, C. Bouzat, S. M. Sine, and R. C. Griggs.** 1996. End-plate acetylcholine receptor deficiency due to nonsense mutations in the ε subunit. Ann. Neurol. **40:**810–817.
13. **Engel, A. G., K. Ohno, and S. M. Sine.** 2003. Sleuthing molecular targets for neurological diseases at the neuromuscular junction. Nat. Rev. Neurosci. **4:**339–352.
14. **Engel, A. G., and S. M. Sine.** 2005. Current understanding of congenital myasthenic syndromes. Curr. Opin. Pharmacol. **5:**308–321.
15. **Escher, P., E. Lacazette, M. Courtet, A. Blindenbacher, L. Landmann, G. Bezakova, K. C. Lloyd, U. Mueller, and H. R. Brenner.** 2005. Synapses form in skeletal muscles lacking neuregulin receptors. Science **308:**1920–1923.
16. **Fatt, P., and B. Katz.** 1952. Spontaneous subthreshold activity at motor nerve endings. J. Physiol. **117:**109–128.
17. **Fromm, L., and S. J. Burden.** 2001. Neuregulin-1-stimulated phosphorylation of GABP in skeletal muscle cells. Biochemistry **40:**5306–5312.

18. **Fromm, L., and S. J. Burden.** 1998. Synapse-specific and neuregulin-induced transcription require an Ets site that binds GABPα/GABPβ. Genes Dev. **12:**3074–3083.
19. **Hwang, S. Y., P. J. Hertzog, K. A. Holland, S. H. Sumarsono, M. J. Tymms, J. A. Hamilton, G. Whitty, I. Bertoncello, and I. Kola.** 1995. A null mutation in the gene encoding a type I interferon receptor component eliminates antiproliferative and antiviral responses to interferons alpha and beta and alters macrophage responses. Proc. Natl. Acad. Sci. USA **92:**11284–11288.
20. **Kandel, E. R., and S. A. Siegelbaum.** 2000. Signalling at the nerve-Muscle synapse: directly gated transmission, p. 196–197. *In* E. R. Kandel, J. H. Schwartz, and T. M. Jessell (ed.), Principals of neural science, 4th ed. McGraw-Hill Publishers, New York, NY.
21. **Khurana, T. S., A. G. Rosmarin, J. Shang, T. O. B. Krag, S. Das, and S. Gammeltoft.** 1999. Activation of utrophin promoter by heregulin via the *ets*-related transcription factor complex GA-binding protein α/β. Mol. Biol. Cell **10:**2075–2086.
22. **Knight, D., L. K. Tolley, D. K. Kim, N. A. Lavidis, and P. G. Noakes.** 2003. Functional analysis of neurotransmission at β2-laminin deficient terminals. J. Physiol. **3:**789–800.
23. **Koike, S., L. Schaeffer, and J.-P. Changeux.** 1995. Identification of a DNA element determining synaptic expression of the mouse acetylcholine receptor δ-subunit gene. Proc. Natl. Acad. Sci. USA **92:**10624–10628.
24. **Lahoud, M. H., S. Ristevski, D. J. Venter, L. S. Jermiin, I. Bertoncello, S. Zavarsek, S. Hasthorpe, J. Drago, D. de Kretser, P. J. Hertzog, and I. Kola.** 2001. Gene targeting of Desrt, a novel ARID class DNA-binding protein, causes growth retardation and abnormal development of reproductive organs. Genome Res. **11:**1327–1334.
25. **LaMarco, K., C. C. Thompson, B. P. Byers, E. M. Walton, and S. L. McKnight.** 1991. Identification of Ets- and Notch-related subunits in GA binding protein. Science **253:**789–792.
26. **Le Treut, T., J. L. Boudier, E. Jover, and P. Cau.** 1990. Localization of voltage-sensitive sodium channels on the extrasynaptic membrane surface of mouse skeletal muscle by autoradiography of scorpion toxin binding sites. J. Neurocytol. **19:**408–420.
27. **Martin, A. R.** 1976. The effect of membrane capacitance on non-linear summation of synaptic potentials. J. Theoret. Biol. **59:**179–182.
28. **Miniou, P., D. Tiziano, T. Frugier, N. Roblot, M. Le Meur, and J. Melki.** 1999. Gene targeting restricted to mouse striated muscle lineage. Nucleic Acids Res. **27:**i–iv.
29. **Missias, A. C., G. C. Chu, B. J. Klocke, J. R. Sanes, and J. P. Merlie.** 1996. Maturation of the acetylcholine receptor in skeletal muscle: regulation of the AChR γ-to-ε switch. Dev. Biol. **179:**223–238.
30. **Nichols, P., R. Croxen, A. Vincent, R. Rutter, M. Hutchinson, J. Newsom-Davis, and D. Beeson.** 1999. Mutation of the acetylcholine receptor ε-subunit promoter in congenital myasthenic syndrome. Ann. Neurol. **45:**439–443.
31. **Nicole, S., B. Desforges, G. Millet, J. Lesbordes, C. Cifuentes-Diaz, D. Vertes, M.-L. Cao, F. De Backer, L. Languille, N. Roblot, V. Joshi, J.-M. Gillis, and J. Melki.** 2003. Intact satellite cells lead to remarkable protection against Smn gene defect in differentiated skeletal muscle. J. Cell Biol. **161:**571–582.
32. **Ohno, K., B. Anlar, and A. G. Engel.** 1999. Congenital myasthenic syndrome caused by a mutation in the Ets-binding site of the promoter region of the acetylcholine receptor ε subunit gene. Neuromuscular Disorders **9:**131–135.
33. **Ohno, K., A. G. Engel, X. M. Shen, D. Selcen, J. Brengman, C. M. Harper, A. Tsujino, and M. Milone.** 2002. Rapsyn mutations in humans cause endplate acetylcholine-receptor deficiency and myasthenic syndrome. Am. J. Hum. Genet. **70:**875–885.
34. **Ohno, K., P. A. Quiram, M. Milone, H.-L. Wang, M. C. Harper, J. N. Pruitt II, J. M. Brengman, L. Pao, K. H. Fischbeck, T. O. Crawford, S. M. Sine, and A. G. Engel.** 1997. Congenital myasthenic syndromes due to heteroallelic nonsense/missense mutations in the acetylcholine receptor ε subunit gene: identification and functional characterization of six new mutations. Hum. Mol. Genet. **6:**753–766.
35. **Ristevski, S., D. A. O'Leary, A. P. Thornell, M. J. Owen, I. Kola, and P. J. Hertzog.** 2004. The ETS transcription factor *Gabpα* is essential for early embryogenesis. Mol. Cell. Biol. **24:**5844–5849.
36. **Robinson, J.** 1976. Estimation of parameters for a model of transmitter release at synapses. Biometrics **32:**61–68.
37. **Sanij, E., T. Hatzistavrou, P. Hertzog, I. Kola, and E. J. Wolvetang.** 2001. Ets-2 is induced by oxidative stress and sensitizes cells to H_2O_2-induced apoptosis: implications for Down's syndrome. Biochem. Biophys. Res. Commun. **287:**1003–1008.
38. **Scarpulla, R. C.** 2002. Transcriptional activators and coactivators in the nuclear control of mitochondrial function in mammalian cells. Gene **286:**81–89.
39. **Schaeffer, L., A. de Kerchove d'Exaerde, and J.-P. Changeux.** 2001. Targeting transcription to the neuromuscular synapse. Neuron **31:**15–22.
40. **Schaeffer, L., N. Duclert, M. Huchet-Dymanus, and J.-P. Changeux.** 1998. Implication of a multisubunit Ets-related transcription factor in synaptic expression of the nicotinic acetylcholine receptor. EMBO J. **17:**3078–3090.
41. **Sternberg, N., and D. Hamilton.** 1981. Bacteriophage P1 site-specific recombination—recombination between *lox*P sites. J. Mol. Biol. **150:**467–486.
42. **Vincent, A., C. Newland, R. Croxen, and D. Beeson.** 1997. Genes at the junction—candidates for congenital myasthenic syndromes. Trends Neurosci. **20:**15–22.
43. **Witzemann, V., H. Schwarz, M. Koenen, C. Berberich, A. Villarroel, A. Wernig, H. R. Brenner, and B. Sakmann.** 1996. Acetylcholine receptor ε-subunit deletion causes muscle weakness and atrophy in juvenile and adult mice. Proc. Natl. Acad. Sci. USA **93:**13286–13291.